Genetic Algorithm Optimization of Bi-phase Codes: Surpassing Barker Code Performance in ISAC Applications

Sevda Şahin
S2 System Engineering
Voorschoten, The Netherlands
e-mail: sevda.sahin@s2system.nl

Tolga Girici
Faculty of Science and Technology
Middlesex University, NW4 4BT
London, United Kingdom
e-mail: t.girici@mdx.ac.uk

***Abstract*—This paper formalizes the ambiguity function for bi-phase coded waveforms in Integrated Sensing and Communication (ISAC) systems. Utilizing a generalized formula, this study optimizes the Peak to Side Lobe Ratio (PSLR) through a genetic algorithm, enhancing both radar and communication performances simultaneously. The optimized codes show substantial improvements in detection and transmission capabilities using traditional Barker codes, validating the proposed method's efficacy. These results highlight the potential of bi-phase codes to revolutionize ISAC technologies by effectively balancing dual-function requirements.**

Keywords-Barker code; Integrated Sensing and Communication (ISAC); Symbol Error Rate (SER); waveform design; Genetic Algorithm

I. INTRODUCTION

The ISAC concept has become quite popular in recent years, aiming to address issues such as spectrum congestion resulting from the increasing variety of both military and civilian wireless communication products, and electromagnetic interference problems on platform installations. Various studies in the literature aim to solve all these problems [1]. However, radar and communication systems process information in different ways. While radar systems extract information from observations gathered in noisy environments, communication systems focus on transmitting predefined signals and extracting information from the noisy environment on the receiver's side. ISAC aims to combine these two functions to achieve a balanced performance through trade-offs [1]–[3]. These studies are generally categorized into two groups: sensing using communication signals and communication using sensing signals. In ISAC studies focusing on communication signals, Orthogonal Frequency Division hlMultiplexing (OFDM) signals are frequently used for sensing over communication signals [4], [5]. However, when OFDM signals are used for radar detection, the bandwidth required for the radar's high range resolution is greater than that of a typical communication data link. In this case, high-sampling-rate Analog-to-Digital Converters (ADC) and thus high-cost hardware must be incorporated into the system. Other communication signals, such asOrthogonal Chirp-Division Multiplexing (OCDM) and Orthogonal Time-Frequency Space (OTFS), have also been studied [4], [6]. All of these multi-carrier communication signals must support full-duplex operation when used for target detection in a mono-static scenario. In this case, ensuring complete isolation between the receiver and transmitter while maintaining receiver sensitivity and dynamic range presents a separate design challenge. Within the scope of communication over sensing signals, Linear Frequency Modulated (LFM) radar signals have been recommended in [7], [8] and phase coded waveforms has been recommended in [9] for transmitting communication signals. In order to evaluate the radar performance (e.g., range and Doppler resolution) of the proposed waveforms for ISAC systems, it is useful to mathematically formulate and analyze the ambiguity functions. In [10], the optimized OTFS waveform is proposed as an ISAC waveform, and ambiguity function analyses have been conducted. In [11], Hyperbolic Fractional Fourier Transform (HFrFT) multicarrier signals have been applied to ISAC systems, and their performance has been analyzed using the ambiguity function. In [12], the authors design integrated radar and communication systems using weighted pulse trains with Oppermann sequences, deriving an analytical expression for the ambiguity function and showing that it depends on a single sequence parameter, thus simplifying the design process. In [13], the authors demonstrate that embedding Phase-Shift Keying (PSK) symbols in radar waveforms can benefit both radar and communication in a dual system, showing that PSK modulation reduces ambiguity function sidelobe peaks and increases the number of orthogonal transmit waveforms without raising sidelobe levels. In [14], the authors use a genetic algorithm to Optimize Code-shift Keying (CSK) sequences in a Frequency Hopping (FH) MIMO radar system, analyzing the ambiguity function with and without information symbol embedding. The optimized sequences significantly reduce range sidelobe levels and clutter modulation, addressing challenges from hopping frequency re-use, while also providing good spectrum containment and supporting high communication data rates. Despite not using the ambiguity function, the authors in [15] focus on the simultaneous optimization of autocorrelation and cross-correlation characteristics of Oppermann sequences as a multiobjective problem. They evaluate the performance of various state-of-the-art multiobjective evolutionary meta-heuristic algorithms for designing Oppermann sequences in integrated radar and communication systems.

In this study, we contribute to the literature by mathematically formulating the ambiguity functions for pulsed ISAC-Barker waveforms, as proposed in our previous work [9]. This formulation takes into account the matched filter bank structure at the radar receiver, as detailed in our recent study [16]. The resulting expressions provide a general framework applicable

to biphase-coded sequences.

Additionally, the ambiguity functions for zero-delay and zero-Doppler cuts are plotted and compared both theoretically and through signal simulations. Subsequently, an analysis of the PSLR for the zero delay and zero Doppler cuts of the uncertainty function of the ISAC-Barker waveform was conducted. The target detection performance in radar functionality is directly related to the PSLR. On the other hand, the distance between symbols directly affects the SER performance of the communication function. In this study, the objective function was defined using the peak-to-sidelobe ratio values of the ambiguity function at the zero Doppler and zero delay cross sections, along with the Hamming distances of the codes. Optimal codes were generated for various lengths and symbol counts using a genetic algorithm. Additionally, a global optimization was performed, taking into account not only the zero Doppler and zero delay cross sections but all cross sections of the ambiguity function. The radar and communication performances of the ISAC system were evaluated for both the codes generated as a result of the optimization and for Barker codes.

The remainder of this paper is organized as follows. In Section II, the signal model and ambiguity function formulation for pulsed ISAC waveforms are presented. Section III describes the design of biphase-coded sequences using a genetic algorithm, including the dual-objective optimization framework. Section IV provides numerical results, comparing the performance of the optimized binary sequences with conventional Barker codes in terms of PSLR and SER. Finally, Section V concludes the paper with a summary of the contributions and a discussion of potential future work.

II. Ambiguity Function

The radar ambiguity function represents the output of the matched filter and describes the interference caused by a target's range and/or Doppler shift compared to a reference target with the same RCS (Radar Cross Section). The ambiguity function calculated at $(\tau, f_d) = (0, 0)$ corresponds to the matched filter output that perfectly matches the signal reflected from the target of interest. In other words, the reflections from the nominal target are located at the origin of the ambiguity function. Therefore, the ambiguity function values at non-zero τ and f_d represent reflections related to different ranges and Doppler shifts from those of the nominal target [17]. For a moving target, the output of the matched filter is calculated as given in (1). Here, f_d represents the Doppler frequency.

$$\chi(\tau, f_d) = \int_{-\infty}^{\infty} \tilde{x}(t)\tilde{x}^*(t-\tau)e^{j\pi f_d t}dt \tag{1}$$

The square of the absolute value of the matched filter output yields the ambiguity function given in (2).

$$|\chi(\tau, f_d)|^2 = \left| \int_{-\infty}^{\infty} \tilde{x}(t)\tilde{x}^*(t-\tau)e^{j\pi f_d t}dt \right|^2 \tag{2}$$

The radar ambiguity function is used by radar designers to examine different waveforms. The suitability of various radar waveforms for different radar applications can be analyzed using the ambiguity function. It is also used to determine the range and Doppler resolutions for a specific radar waveform. A three-dimensional plot of the ambiguity function against frequency and time delay is referred to as the radar ambiguity diagram [17].

A. Barker-Coded ISAC Joint Waveform Ambiguity Function

In this work, the term *joint waveform refers to a waveform that simultaneously performs radar sensing and communication functions. The joint waveform is generated according to the method defined in [9]. This allows the radar pulse to carry information for the communication receiver while retaining its radar sensing properties. While the fundamental ambiguity function for pulsed phase-coded waveforms is well-established in classical radar theory [17], the formulation presented here explicitly extends these results to ISAC-Barker joint waveforms with multiple communication symbols and pulse sequences, providing a practical framework for subsequent optimization analyses. The complex envelope of a single phase-coded pulse is expressed as*,

$$x_1(t) = e^{jw_0 t} \sum_{n=1}^{N} P_n(t) e^{j\theta_n}. \tag{3}$$

Where w_0 denotes the carrier angular frequency of the pulse and $P_n(t)$ represents the n-th sub-pulse envelope. When a binary phase code is used, θ_n is either 0 or π. Each sub-pulse is modulated in phase according to the corresponding phase code $D_n = e^{j\theta_n} = \pm 1$ for a bi-phase Barker code. Specifically, the transmitted waveform can be expressed as a sum of phase-coded sub-pulses, where D_n multiplies $P_n(t)$ to impose the desired phase shift. For the joint waveform, D_n changes in accordance with the transmitted communication symbol. Since the Barker code is a bi-phase code, the ambiguity function of a Barker-coded pulse for $0 < \tau < N\tau_0$ is expressed by (4) [17].Where τ_0 is a single sub-pulse with duration.

$$\begin{aligned} \chi_{ISAC-Barker}(\tau, f_d) = & \\ & \chi_0(\tau', f_d) \sum_{n=1}^{M-k} D_n D_{n+k} e^{-j2\pi f_d (n-1)\tau_0} \\ & + \chi_0(\tau_0 - \tau', f_d) \sum_{n=1}^{M-k} D_n D_{n+k+1} e^{-j2\pi f_d n \tau_0} \end{aligned} \tag{4}$$

Here, M is number of communication symbols, τ is given in (5), and $\chi_0(\tau', f_d)$ is given in (6).

$$\tau = k\tau_0 + \tau' \begin{cases} 0 < \tau' < \tau_0 \\ k = 0, 1, 2, ..., M \end{cases} \tag{5}$$

$$\chi_0(\tau', f_d) = \int_0^{\tau_0 - \tau'} e^{-j2\pi f_d t} dt, 0 < \tau' < \tau_0 \tag{6}$$

For a sequence of L pulses,each consisting of N sub-pulses, with Pulse Repetition Interval (PRI) T, where the complex envelope of a single pulse is given by (3), the transmitted

signal consisting of L consecutive pulses is expressed as in (7).

$$\tilde{x}_{LT}(t) = \frac{1}{\sqrt{L}} \sum_{i=0}^{L-1} \tilde{x}_1(t - iT) \tag{7}$$

Where $\tilde{x}_1(t)$ represents the transmitted phase-coded pulse corresponding to the complex envelope $x_1(t)$ in (3).The ambiguity function for a sequence of L pulses is given in (8).

$$|\chi_{LT}(\tau, f_d)| = \frac{1}{L} \sum_{q=-(L-1)}^{L-1} |\chi_1(\tau - qT, f_d)| \times \left| \frac{\sin[\pi f_d (L - |q|)T]}{\sin(\pi f_d T)} \right|, |\tau| \leq LT \tag{8}$$

As proven in [18], the ambiguity function for a sequence of L pulse can be expressed as given in (9) for $|\tau| \leq \tau_0$. This form results from the linearity of the matched filter and the periodic structure of the pulse sequence, where the total ambiguity function is obtained as a weighted sum of the individual pulse ambiguity functions, accounting for Doppler-induced phase shifts.

$$|\chi_{LT}(\tau, f_d)| = |\chi_1(\tau, f_d)| \left| \frac{\sin[\pi f_d LT]}{N \sin(\pi f_d T)} \right| \tag{9}$$

Using (8), the ambiguity function for a sequence of L ISAC-Barker pulses is expressed by (10).

$$|\chi(\tau, f_d)| = \frac{1}{L} \sum_{q=-(L-1)}^{L-1} |\chi_{ISAC-Barker}(\tau - qT, f_d)| \times \left| \frac{\sin[\pi f_d LT]}{\sin(\pi f_d T)} \right|, |\tau| \leq LT \tag{10}$$

Using (9) and (10), the ambiguity function for a sequence of L ISAC-Barker pulses can be calculated for $|\tau| \leq \tau_0$ as shown in (11).

$$|\chi(\tau, f_d)| = |\chi_{ISAC-Barker}(\tau, f_d)| \left| \frac{\sin[\pi f_d LT]}{N \sin(\pi f_d T)} \right|, |\tau| \leq \tau_0 \tag{11}$$

In (12), the zero-Doppler cut for a pulse sequence with the ISAC-Barker waveform for $|\tau| \leq \tau_0$ is provided.

$$\begin{aligned} &|\chi(\tau, 0)| \\ &= \lim_{f_d \to 0} \frac{1}{L} \sum_{q=-(L-1)}^{L-1} |\chi_{ISAC-Barker}(\tau - qT, f_d)| \times \left| \frac{\sin[\pi f_d LT]}{L \sin(\pi f_d T)} \right| \\ &= \frac{1}{L} \sum_{q=-(L-1)}^{L-1} |\chi_{ISAC-Barker}(\tau - qT, 0)| \\ &= \frac{1}{L} \sum_{q=-(L-1)}^{L-1} ((\tau_0 - \tau' + qT) \sum_{n=1}^{N-k} D_n D_{n+k} + (\tau' + qT) \sum_{n=1}^{N-k} D_n D_{n+k+1}) \end{aligned} \tag{12}$$

The locations of the peaks on the delay axis at the zero Doppler cross-section depend on the PRI of the pulse sequence, regardless of the waveform. In this context, the function given by (12), which describes the zero-Doppler cut for a pulse sequence with the ISAC-Barker waveform, exhibits its first peak at $\tau = 0$. Other peaks are observed at $\tau = (n-1)T$ for $n = 1, ..., L$. The widths of all peaks are $2\tau_c$, where $\tau_c = 1/B$ as stated in [17]. The peak values depend only on the number of pulses L in the sequence and are given by $(L - (n-1))/L$. The zero-delay cut for a pulse sequence with the ISAC-Barker waveform is,

$$\begin{aligned} &\chi_{ISAC-Barker}(0, f_d) \\ &= \left(\chi_0(0, f_d) \sum_{n=1}^{N-k} D_n D_{n+k} e^{-j2\pi f_d (n-1)\tau_0} + \chi_0(\tau_0, f_d) \sum_{n=1}^{N-k} D_n D_{n+k+1} e^{-j2\pi f_d n \tau_0} \right) \\ &\quad \times \left| \frac{\sin[\pi f_d (L - |q|)T]}{\sin(\pi f_d T)} \right|. \end{aligned} \tag{13}$$

The locations of the peak values on the Doppler frequency axis at the zero-delay cross-section depend on the PRI of the pulse sequence, regardless of the waveform, and the peak values are observed at integer multiples of $f_d = 1/T$. The widths of peaks are $2/LT$ [19]. The peak values are given by $\frac{\sin[\pi(k/T)\tau_0]}{\pi(k/T)} \tau_0$, where k is a positive integer.

Figure 1 shows the normalized Doppler cut and the normalized delay cut for ISAC-Barker waveforms with L pulses. As can be seen from the zoomed in section of the graph in Figure 1, the PSLR for the ISAC-Barker waveform is approximately 4 (12 dB). This situation is considered to cause erroneous range measurements for the ISAC-Barker waveform, especially in reflections from nearby targets. At this stage of the study, a genetic algorithm was used to generate an optimal binary phase-coded waveform, in order to reduce the observed PSLR in the ISAC-Barker waveform as proposed in [14].

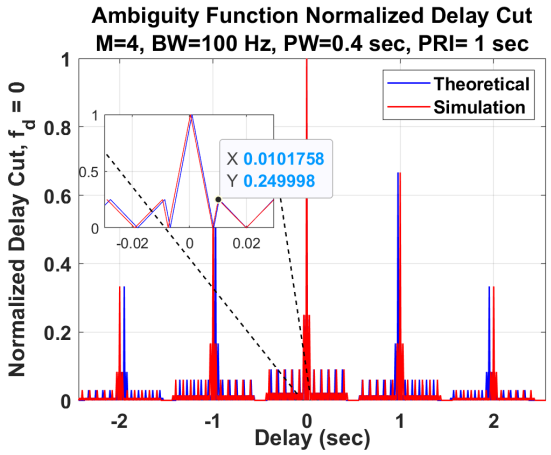

(a) Delay cut

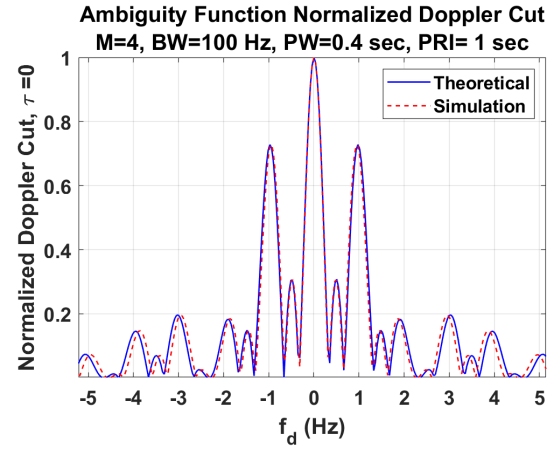

(b) Doppler cut

Figure 1. Ambiguity function cuts for ISAC-Barker waveform. (a) Delay cut. (b) Doppler cut.

III. Biphase Sequence Optimization by Using Genetic Algorithm

In Section II, the ambiguity function we derived for an ISAC system with pulsed waveforms coded with Barker codes within a pulse is applicable to all biphase phase codes. Motivated by this generalization, we employ a genetic algorithm to design alternative biphase-coded sequences with improved performance. The sequence design problem is discrete, highly non-convex, and involves a large combinatorial search space. Furthermore, the optimization targets multiple conflicting objectives, namely minimizing the PSLR while maintaining reliable communication performance in terms of Hamming distance. Genetic algorithms are well suited for such problems as they efficiently explore large search spaces without requiring gradient information and naturally support multi-objective optimization. In implementing the genetic algorithm, we define two types of objective (fitness) functions. The first function aims to optimize radar performance by maximizing the PSLR at the zero-delay ($PSLR_{Zdel}$), and zero-Doppler ($PSLR_{Zdopp}$) cuts, while also optimizing the Hamming distance, d_{min}, between communication symbols to optimize communication performance (14).

TABLE I. Genetic Algorithm Parameters

Parameter	N44M4	N88M8
Population Size	40	140
Number of Generations	100	100
Crossover Fraction	0.8	0.8
Elite Count	5	5
Population Type	bitstring	bitstring

$$f_{ZeroCut} = \frac{w_1 M}{N} PSLR_{Zdel} - \frac{w_2 M}{N} PSLR_{Zdopp} + \frac{w_3}{N} d_{min} \quad (14)$$

where N is the code length and M is the number of symbols. The second objective function aims to optimize radar performance by maximizing the first peak-to-second peak ratio, PR_{Global}, in all delay and Doppler cuts, while also maximizing the Hamming distance, d_{min}, between communication symbols to optimize communication performance (15).

$$f_{Global} = \frac{w_1 M}{N} PR_{Global} + \frac{w_3}{N} d_{min} \quad (15)$$

Here w_1, w_2 and w_3 are binary coefficients to emphasize different components of the fitness function. In both objective functions, PLSR computation is performed according to the ambiguity function given in (10). A genetic algorithm is used with the parameters given in Table I. In addition, the best fitness value is plotted at each iteration to monitor optimization progress. For k bit/pulse communications, $M = 2^k$ biphase codes are needed. A random candidate solution can be formed by concatenating M random binary codes. The genetic algorithm is initialized by generating a number of these candidate solutions, each of which is of length NM. Then, fitness evaluation, selection, crossover, mutation and replacement procedures are repeated until a converge criterion is met. MATLAB Global Optimization Toolbox is used in implementing the genetic algorithm.

IV. Numerical Analysis

We initially performed our analysis using sequences of length $N = 44$ with $M = 4$ communication symbols (2 bits per pulse repetition interval). The optimization results demonstrated significant improvements in performance compared to the Barker code. Specifically, the optimized biphase sequences achieved better PSLR for zero Doppler cuts while maintaining competitive Hamming distances.

Key observations for $N = 44, M = 4$ include:

- The PSLR for zero Doppler cut was consistently reduced in the optimized codes, as shown in Table II.
- Adjusting the weights (w_1, w_2, and w_3) allowed for trade-offs between PSLR and minimum Hamming distance, leading to sequences tailored for specific design goals.

Encouraged by the promising results for $N = 44, M = 4$, we extended our analyses to longer sequences and more communication symbols. Building on the success of the $N = 44, M = 4$ case, we repeated the analyses with sequences of length $N = 88$ and $M = 8$ communication symbols (i.e. 3 bits/PRI). The objective was to evaluate whether the observed improvements could be replicated with longer sequences and higher symbol counts.

Similar to the $N = 44, M = 4$ case, the optimized sequences for $N = 88, M = 8$ showed enhanced PSLR for zero Doppler cuts while achieving competitive or better minimum Hamming distances. Key findings include:

- The PSLR improvements in the optimized codes were more pronounced for the zero Doppler case, as seen in Table II.
- The flexibility provided by the objective function weights enabled the design of sequences that balance PSLR and Hamming distance effectively.

To demonstrate the difference in radar performance between the Barker and optimized codes through the ambiguity function graph, the analyses provided in Table II for the $N = 44$, $M = 4$ case are illustrated with ambiguity function and contour plots for the Barker and optimized codes in Figure 2 and Figure 3, respectively. As seen in Figure 2, the Barker code exhibits higher side lobes in the zero-Doppler and zero-delay cuts, which may lead to erroneous target detection or range estimation. In contrast, Figure 3 shows that the optimized biphase code suppresses these side lobes, resulting in a cleaner main peak and reduced ambiguity. This clearly demonstrates the improvement in radar resolution and potential communication reliability achieved by the genetic algorithm-optimized codes.

After analyzing the radar performance of these codes, we also evaluated the SER performance of each code for a communication receiver using correlation [9], as illustrated in Figure 4. The SER graphs show how the optimized codes outperform the Barker code in terms of symbol detection accuracy under the same Signal-to-Noise Ratio (SNR) conditions. Since our communication system performs demodulation using correlation, the autocorrelation and cross-correlation characteristics of the waveforms play a significant role in the symbol error rate. The optimized codes have better autocorrelation performance compared to the Barker code because their side lobes are suppressed. As a result, as shown in the SER graphs, the communication performance of the optimized codes is significantly better than that of the Barker code for both $N = 44, M = 4$ and $N = 88, M = 8$. While the analysis emphasizes zero-Doppler and zero-delay cuts, it is important to evaluate the performance under high Doppler shifts, which are relevant in high-mobility scenarios such as automotive or surveillance ISAC applications. Future work should include analyzing the ambiguity function and PSLR for significant Doppler frequencies to assess the robustness of the optimized biphase codes in such environments.

When analyzing the SER performance for the three different optimization objective (Global, Zero Cut with $w_1 = 1, w_2 = 1, w_3 = 1$, and Zero Cut with $w_1 = 1, w_2 = 1, w_3 = 0$), we observe that the results are very similar for both $N = 44, M = 4$ and $N = 88, M = 8$. The SER performance for these optimization objectives is almost identical, with only minor differences at lower SNR levels, as can be seen in the Figure 4. It should be noted that the current SER evaluations assume ideal AWGN channels. The robustness of the proposed codes under practical channel conditions—including multipath fading, frequency selectivity, and hardware impairments—remains an important direction for future investigation.

TABLE II. PSLR AND HAMMING DISTANCE FOR OPTIMIZED AND BARKER CODES. PSLR IS COMPUTED FOR ZERO DOPPLER AND ZERO DELAY CUTS OF THE AMBIGUITY FUNCTION. HAMMING DISTANCE INDICATES THE MINIMUM DISTANCE BETWEEN CODEWORDS.

Code	PSLR Zero Doppler	PSLR Zero Delay	Hamming Distance
Barker44M4	4.0000	4.6031	22
N44M4W111ZC	4.8889	4.6031	22
N44M4W110ZC	5.5000	4.6031	20
N44M4W111G	4.0000	4.6031	25
Barker88M8	4.0000	4.6040	44
N88M8W111ZC	6.2857	4.6040	44
N88M8W110ZC	6.7692	4.6040	37
N88M8W111G	5.5000	4.6040	46

This similarity in SER performance of the optimized sequences can be attributed to the fact that the autocorrelation and cross-correlation characteristics of the optimized sequences are similar. The suppression of side lobes in these sequences leads to similar autocorrelation properties, which, in turn, results in comparable performance when the demodulation is performed using correlation-based methods.

In this study, nested Barker sequences are selected as the primary baseline due to their well-known ambiguity function characteristics, low implementation complexity, and frequent use in pulsed radar waveform designs. While other sequence families such as Zadoff-Chu, Golay, and Gold sequences are typically designed under different signal structure assumptions, such as constant-envelope transmission or complementary coding, which can be used to design an ISAC waveform. A comprehensive performance comparison with these advanced sequence families is considered an important direction for future work.

V. CONCLUSION AND FUTURE WORK

In this study, we considered a usage concept where both radar and communication functions can be realized using a joint waveform in ISAC systems. We used pulsed signals with Barker intra-pulse modulation as the ISAC joint waveform. After mathematically expressing the ambiguity function of the ISAC-Barker waveform, we performed ambiguity function analyses using both mathematical expressions and signal simulations. We observed that the PSLR of the $B44$ Barker sequences we proposed for $M = 4$ is somewhat lower compared to the optimized biphase codes under the same Pulse Width (PW), PRI, and bandwidth conditions.

Furthermore, we performed optimizations to improve the communication performance by using biphase codes. Specifi-

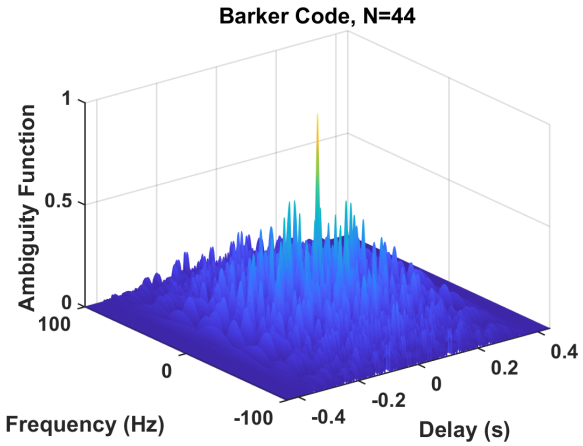

(a) Ambiguity function

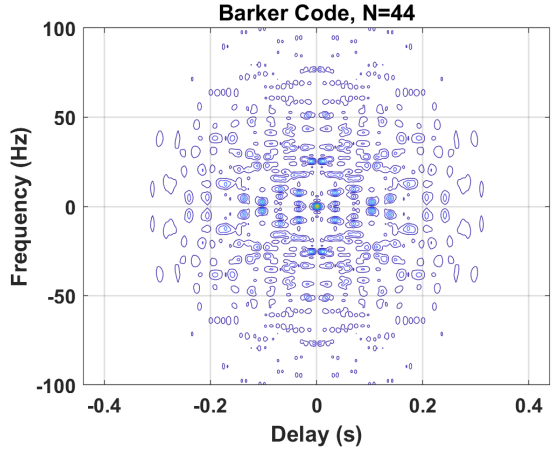

(b) Contour plot for the Barker code (N=44)

Figure 2. (a) Ambiguity function. (b) Contour plot for the Barker code (N=44).

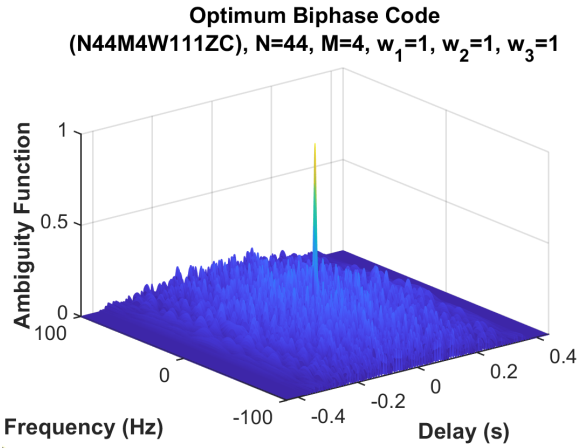

(a) Ambiguity function

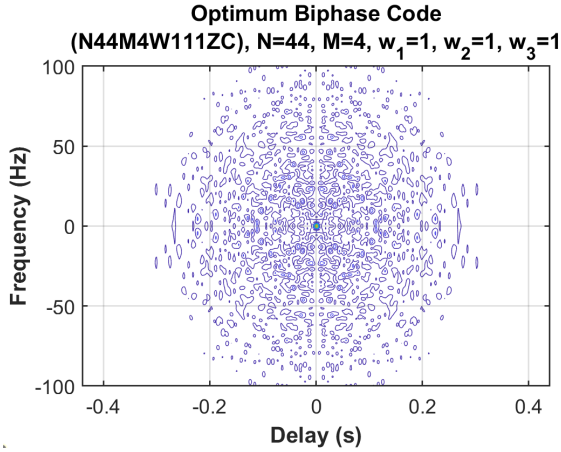

(b) Contour plot for the optimum biphase code, $w_1 = 1$, $w_2 = 1$, $w_3 = 1$ (N=44, M=4)

Figure 3. (a) Ambiguity function. (b) Contour plot for the optimum biphase code, $w_1 = 1$, $w_2 = 1$, $w_3 = 1$ (N=44, M=4).

cally, we applied genetic algorithms to optimize the codes for different objective functions: Zero Cut, and Global optimization. We compared the results of these optimized codes to the traditional nested Barker code. The optimization led to significant improvements in the side lobe suppression, which in turn enhanced the radar performance as well as the communication performance.

When analyzing the SER for the optimized codes, we observed that their performance was notably better than the Barker code, especially in terms of autocorrelation and cross-correlation characteristics. The optimized codes exhibited better autocorrelation properties, resulting in reduced side lobes and improved communication performance. However, the SER performance of the three optimization schemes (Global, Zero Cut with $w_1 = 1, w_2 = 1, w_3 = 1$, and Zero Cut with $w_1 = 1, w_2 = 1, w_3 = 0$) was found to be very similar for both $N = 44, M = 4$ and $N = 88, M = 8$ codes. Minor differences in performance were observed only at lower SNR levels. The optimized sequences demonstrate improved SER performance compared to the Barker code, due to their enhanced autocorrelation and cross-correlation characteristics.

It is important to emphasize that the communication-over-sensing paradigm considered in this work is not primarily intended for high-throughput data transmission, as targeted in enhanced mobile broadband scenarios. Instead, the main objective is to preserve sensing performance while enabling reliable exchange of sensing-related information, such as target detection results, tracking data, and control or coordination messages among distributed sensing nodes. Within this operational concept, relatively low data rates (e.g., 2–3 bits per Pulse Repetition Interval) are sufficient.

Future research can investigate the extension of the optimization to multi-level phase codes, which may provide further improvements in radar and communication performance.

In conclusion, the optimization of biphase codes led to improved radar and communication performance compared to the nested Barker code. The results demonstrated the effectiveness of the optimization methods in enhancing both the radar and communication capabilities in ISAC systems.

 ISBN: 978-1-68558-360-6

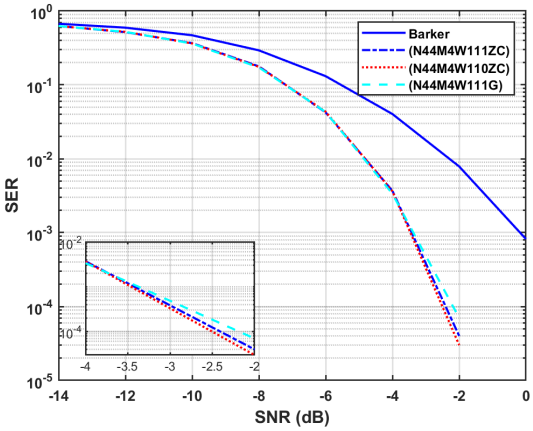

(a) SER $N = 44$, $M = 4$

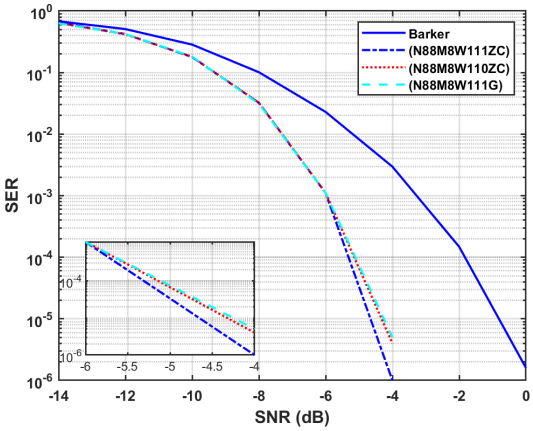

(b) SER $N = 88$, $M = 8$

Figure 4. SER performance for different code lengths and symbol counts.

REFERENCES

[1] F. Liu, C. Masouros, A. P. Petropulu, H. Griffiths, and L. Hanzo, "Joint radar and communication design: Applications, state-of-the-art, and the road ahead", *IEEE Transactions on Communications*, vol. 68, no. 6, pp. 3834–3862, 2020. DOI: 10.1109/TCOMM.2020.2973976.

[2] Y. Cui, F. Liu, X. Jing, and J. Mu, "Integrating sensing and communications for ubiquitous iot: Applications, trends, and challenges", *IEEE Network*, vol. 35, no. 5, pp. 158–167, 2021. DOI: 10.1109/MNET.010.2100152.

[3] Z. Cui, J. Hu, J. Cheng, and G. Li, "Multi-domain noma for isac: Utilizing the dof in the delay-doppler domain", *IEEE Communications Letters*, vol. 27, no. 2, pp. 726–730, 2023. DOI: 10.1109/LCOMM.2022.3228873.

[4] L. Giroto de Oliveira et al., "Joint radar-communication systems: Modulation schemes and system design", *IEEE Transactions on Microwave Theory and Techniques*, vol. 70, no. 3, pp. 1521–1551, 2022. DOI: 10.1109/TMTT.2021.3126887.

[5] D. Garmatyuk, J. Schuerger, and K. Kauffman, "Multifunctional software-defined radar sensor and data communication system", *IEEE Sensors Journal*, vol. 11, no. 1, pp. 99–106, 2011. DOI: 10.1109/JSEN.2010.2052100.

[6] X. Lv, J. Wang, Z. Jiang, and W. Jiao, "A novel papr reduction method for ocdm-based radar-communication signal", in *2018 IEEE MTT-S International Microwave Workshop Series on 5G Hardware and System Technologies (IMWS-5G)*, 2018, pp. 1–3. DOI: 10.1109/IMWS-5G.2018.8484372.

[7] M. B. Alabd, L. G. de Oliveira, B. Nuss, W. Wiesbeck, and T. Zwick, "Time-frequency shift modulation for chirp sequence based radar communications", in *2020 IEEE MTT-S International Conference on Microwaves for Intelligent Mobility (ICMIM)*, 2020, pp. 1–4. DOI: 10.1109/ICMIM48759.2020.9298987.

[8] S. Jha, N. M. Balasubramanya, B. K. Chalise, and M. G. Amin, "Performance analysis of lora waveform for joint communications and radar system", *IEEE Transactions on Radar Systems*, vol. 1, pp. 243–248, 2023. DOI: 10.1109/TRS.2023.3294799.

[9] S. Şahin and T. Girici, "Phase coded waveforms for integrated sensing and communication systems", *IET Radar, Sonar and Navigation*, 2024. DOI: 10.1049/rsn2.12661.

[10] M. Weiß, "A novel waveform for a joint radar and communication system", in *2022 23rd International Radar Symposium (IRS)*, 2022, pp. 259–263. DOI: 10.23919/IRS54158.2022.9904976.

[11] M. R. Mousavi and S. Ludwig, "Ambiguity function analysis of hyperbolic fractional fourier transform in joint radar and communication applications", in *2024 International Radar Symposium (IRS)*, 2024, pp. 206–211.

[12] M. Jamil, H.-J. Zepernick, and M. I. Pettersson, "On integrated radar and communication systems using oppermann sequences", in *MILCOM 2008 - 2008 IEEE Military Communications Conference*, 2008, pp. 1–6. DOI: 10.1109/MILCOM.2008.4753277.

[13] I. P. Eedara, A. Hassanien, M. G. Amin, and B. D. Rigling, "Ambiguity function analysis for dual-function radar communications using psk signaling", in *2018 52nd Asilomar Conference on Signals, Systems, and Computers*, 2018, pp. 900–904. DOI: 10.1109/ACSSC.2018.8645328.

[14] I. P. Eedara, M. G. Amin, and A. Hoorfar, "Optimum code design using genetic algorithm in frequency hopping dual function mimo radar communication systems", in *2020 IEEE Radar Conference (RadarConf20)*, 2020, pp. 1–6. DOI: 10.1109/RadarConf2043947.2020.9266623.

[15] M. Jamil, H.-J. Zepernick, and X.-S. Yang, "Sequence optimization for integrated radar and communication systems using meta-heuristic multiobjective methods", in *2017 IEEE Radar Conference (RadarConf)*, 2017, pp. 502–507. DOI: 10.1109/RADAR.2017.7944255.

[16] S. Şahin and T. Girici, "A novel radar receiver for joint radar and communication systems", in *2023 International Conference on Radar, Antenna, Microwave, Electronics, and Telecommunications (ICRAMET)*, 2023, pp. 61–66. DOI: 10.1109/ICRAMET60171.2023.10366608.

[17] B. R. Mahafza, *Radar Signal Analysis and Processing Using Matlab*. Taylor & Francis Group, 2009.

[18] N. Levanon, "The periodic ambiguity function — its validity and value", in *2010 IEEE Radar Conference*, 2010, pp. 204–208. DOI: 10.1109/RADAR.2010.5494626.

[19] A. De Maio and A. Farina, "Waveform diversity: Past, present, and future", *RTO-EN-SET-119*, 2010.